Optical Engineering

SPIEDigitalLibrary.org/oe

Three-dimensional scanning of specular and diffuse metallic surfaces using an infrared technique

Alban Bajard
Olivier Aubreton
Youssef Bokhabrine
Benjamin Verney
Gönen Eren
Aytül Erçil
Frederic Truchetet

SPIE

Three-dimensional scanning of specular and diffuse metallic surfaces using an infrared technique

Alban Bajard
Olivier Aubreton
Youssef Bokhabrine
Benjamin Verney
Laboratoire Le2i
UMR CNRS 6306
12 Rue de la Fonderie
71200 Le Creusot, France
E-mail: alban.bajard@u-bourgogne.fr

Gönen Eren
Galatasaray University
Computer Engineering Department
Ciragan Caddesi 36
Ortakoy, Istanbul 34357, Turkey

Aytül Erçil
Sabanci University
Faculty of Engineering and Natural Sciences
Tuzla, Istanbul 34956, Turkey

Frederic Truchetet
Laboratoire Le2i
UMR CNRS 6306
12 Rue de la Fonderie
71200 Le Creusot, France

Abstract. For the past two decades, the need for three-dimensional (3-D) scanning of industrial objects has increased significantly and many experimental techniques and commercial solutions have been proposed. However, difficulties remain for the acquisition of optically non-cooperative surfaces, such as transparent or specular surfaces. To address highly reflective metallic surfaces, we propose the extension of a technique that was originally dedicated to glass objects. In contrast to conventional active triangulation techniques that measure the reflection of visible radiation, we measure the thermal emission of a surface, which is locally heated by a laser source. Considering the thermophysical properties of metals, we present a simulation model of heat exchanges that are induced by the process, helping to demonstrate its feasibility on specular metallic surfaces and predicting the settings of the system. With our experimental device, we have validated the theoretical modeling and computed some 3-D point clouds from specular surfaces of various geometries. Furthermore, a comparison of our results with those of a conventional system on specular and diffuse parts will highlight that the accuracy of the measurement no longer depends on the roughness of the surface. [DOI: 10.1117/1.OE.51.6.063603]

Subject terms: three-dimensional scanning; infrared; heat transfer; specular surfaces; roughness.

Paper 120165 received Feb. 6, 2012; revised manuscript received Mar. 28, 2012; accepted for publication Apr. 6, 2012; published online Jun. 4, 2012.

1 Introduction

Generally, three-dimensional (3-D) shape acquisition is used in a wide range of applications, such as visualization, medical imaging, measurement, reverse engineering and inspection. Unlike conventional scanners which mainly use the properties of visible light, our work uses the infrared (IR) spectral band that is rarely used in 3-D digitization. Conventional systems are highly dependent on the type of surface that is to be scanned. In fact, physical and geometrical reflection models have been proposed,[1] and three classes of opaque surfaces can be identified: diffuse or even Lambertian surfaces, the reflectance of which is omnidirectional [Fig. 1(a)]; glossy surfaces, the reflectance of which is a combination of a diffuse lobe and a specular lobe [Fig. 1(b)] and ideally specular surfaces [Fig. 1(c)].

Surfaces from class A are the most widely studied. Sansoni[2] recently presented a state-of-the-art unification of active and passive techniques along with a variety of examples and applications. The need for this type of technique has been growing in recent years, especially in industry, where quality plays a more and more important role. In our context, active triangulation methods are probably the most often used methods for measuring accurately the 3-D coordinates of a surface. A review of this technique and an extensive bibliography are given by Chen et al.[3] and Beraldin[4]. Because of this progress, a substantial number of active techniques have been successfully commercialized: a discussion of their performances is exposed by Blais.[5] In spite of these advances, digitization of non-cooperative surfaces is far from being a closed problem. Transmission, specular reflection or refraction of light contradicts the operation of conventional 3-D scanners, based on diffuse components of reflection. One way to circumvent these issues is to change the original surface into a diffuse (class A) surface b mechanical or electrochemical treatment[6] or by the deposit of a thin layer of powder. However, this action involves manual intervention and could pose a risk of damaging the surface. Scanning results of a powdered surface [Fig. 2(a)], raw steel [Fig. 2(b)] and a steel surface with a mirroring layer of alumina [Fig. 2(c)] illustrate this problem. We observe in these figures the distortion of the structured light pattern on the objects (fringes projected by the Steinbichler Comet 5 scanner). The influence of the ambient light and multiple inter-reflections on the specular part result in very poor 3-D acquisition.

Thus, glossy and specular surfaces (class B and C identified in Fig. 1) pose challenging problems for acquisition systems. Ihrke et al.[7] present a review and a classification of experimental approaches for 3-D shape reconstruction of all of the non-cooperative surfaces (specular, transparent, translucent, and dynamic scenes). Among the cited solutions, Park and Kak[8] propose a digitization method for the surfaces of the classes B and C. They object to the basis assumption of an active scanner, considering that a projected point

0091-3286/2012/$25.00 © 2012 SPIE

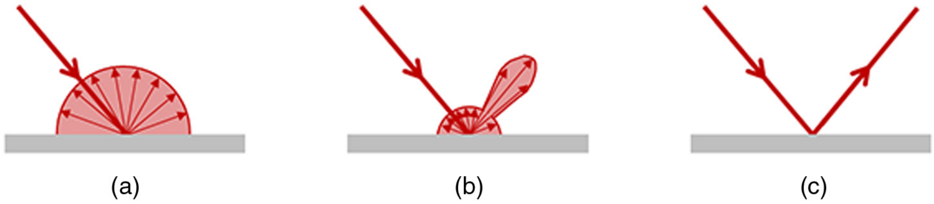

Fig. 1 A classification of reflectance models for opaque surfaces: (a) class A: diffuse surface, (b) class B: glossy surface, (c) class C: specular surface.

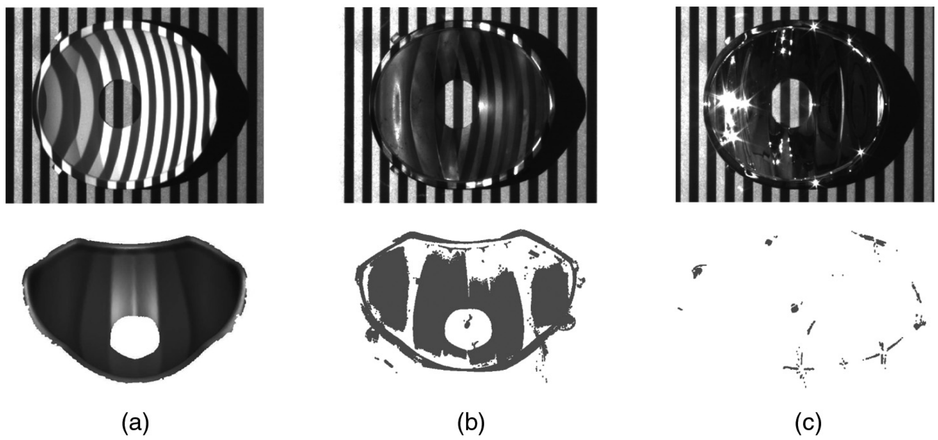

Fig. 2 Distortion of the structured light pattern and the corresponding 3-D digitization results for three types of surfaces: (a) a powdered surface, (b) raw steel, and (c) steel with a mirroring layer of alumina.

orresponds to a single point in the image frame, and they propose to measure all of the points that are reflected by the specular object toward the sensor (results of inter-reflections). Then, the algorithm iteratively removes false points through a series of tests. Because several images have been acquired from different points of view, constraints can be applied to these tests, but the thresholds may need to be defined *a priori*. Although the results allow for a complete visualization of the glossy object, the accuracy is not sufficient for measurement applications or for surface inspection.

Approaches based on "shape from polarization" have also been the topic of many research studies on specular surfaces (and transparent surfaces). Wolff[9] proved the relation between the surface normal and the polarization parameters of the reflected ray at the surface of the material. Then, the technique was extended to specular metallic objects,[10] especially by means of active lighting.[11] Even if the measurement accuracy is good, this method requires a confined environment, which limits the size of the objects that can be reconstructed.

While in the visible range, specular reflections are usually considered to be noise in the reconstruction algorithms, the "Shape from Distortion" techniques can take advantage of specular reflections to compute the depth and orientation of the surface. Tarini et al.[12] were pioneers in "shape from distortion" idea; they proposed to observe the distortion of several light patterns that were projected from a diffuse source (a computer monitor) on the mirroring surface. Bonfort et al.[13] propose a similar method and show that it is possible to recover the shape of specular surfaces by projecting a light pattern from two unknown positions. For these techniques, the cloud of points that is obtained could be very dense, but the matching constraint is high, and an object with a high curvature cannot lead to an entire reconstruction.

Another method, sometimes classified in the "shape from specularities" category, was developed by Zheng et al.[14,15] and has been used widely. The principle relies on the tracking of a specular reflection that is induced by light sources surrounding the object, when the object is rotating. The continuous acquisition by a fixed camera provides a spatiotemporal collection of images. The study of the apparent motion of specular highlights on the object will help to recover the whole surface. However, the authors noted that the reconstruction accuracy depends strongly on the nature of the specular surface. We note that this remark highlights a general drawback to all of the non-conventional techniques that were mentioned above: the presence of any diffuse part on the object will interfere with the cloud of points digitization. In other words, the surfaces of class A or mixed class surfaces cannot be entirely reconstructed by this type of technique.

Other approaches such as multi-camera passive systems,[16] structured-light based systems,[17] or the "shape from fluorescence" technique,[18] have also been proposed, but the accuracy of the measurement is poor, and the surface roughness should not exceed a low bound. Chromatic confocal microscopy[19] is another way to estimate the 3-D coordinates of an opaque surface with good accuracy, but the surface should not be excessively tilted. Some commercial systems mounted on robotic arms[20] operate on the assumption that the reflected radiation at the surface of an object has a quite diffuse component; thus, scanners can acquire a reflective shape after several successive scans if the incident radiation is sufficiently intense and the distance of the measurement is relatively low. However, it appears that no conventional, non-contact technique offers sufficient accuracy and rapidity for an industrial application or can perform fair 3-D measurements on ideal specular surfaces.

Among the non-conventional techniques, the interpretation of thermal images is the subject of some studies, especially in the field of non-destructive testing. Bodnar[21] studied the detection and the dimensional characterization of wear cracks that emerge in metallic materials. The method used is called "photothermal radiometry," and is based on scanning the object with a laser excitation. In the same field, Pelletier and Maldague[22] developed a technique for thermal image analysis called "shape from heating," which can extract the orientation and depth of simple surface (a cylinder in the paper) that is heated by a diffuse IR source. The main goal of this 3-D shape extraction is to improve the detection of defects by correcting the temperature variations that result from the non-planarity of the surface. Even though the accuracy of this method has not been demonstrated yet for the 3-D digitization of complex shapes, this study was among the first to consider thermography to extract 3-D information. More recently, a method is proposed for the calibration of a stereoscopic system that operates in the near IR to combine temperature measurements, 3-D shapes and strain of a metal mold under a heat source.[23] Nevertheless, the matching of stereoscopic images suffers from a lack of texture in the IR images, and the technique is not suitable for specular surfaces (because image correlation becomes more complex).

The studies presented in this article on the 3-D scanning of specular surfaces are related to a nonconventional IR approach introduced by Eren et al.[24] for the 3-D digitization of glass objects. Unlike classical active triangulation approaches, the principle of this technique, called scanning from heating (SFH) is based on the measurement of the IR radiation that is emitted by the object instead of the reflection of visible radiation. A laser source is used to cause a local elevation of temperature; the 3-D coordinates of each point are then extracted from the IR images with a prior geometric calibration of the system. Because the emissivity is omnidirectional for most materials, the model of IR radiation tends to approach the model of the diffuse reflection of visible light for surfaces of class A (see Fig. 1), and thus addresses the issue of specular reflection or transparency in the visible spectrum. Using a CO_2 laser, the feasibility of this concept has been demonstrated on glass objects, and some scanning results have been presented.[25] The challenge of our work is related to the study of the thermal properties of metals that have a high reflectivity and a high thermal conductivity to extend the SFH principle to 3-D acquisition of specular metallic surfaces. The first part presents the physical properties to be considered for the heating process, and a finite element model used for choosing the system settings. In the second part, after explaining the relation between the roughness and the specularity of a surface, we show that in contrast to a conventional system, 3-D scanning results computed by our method do not depend on the roughness. The last section concludes this study and presents directions for future research.

2 Heat Transfer Modeling

2.1 *Theoretical Background*

The characteristics of the laser source used for the heat generation must be chosen in consideration of the thermophysical properties of the studied materials on which the SFH technique will be applied. If the quantity of heat is insufficient, the temperature rise cannot be detected by the thermal sensor. Consequently the surface can be damaged (e.g., by marking, melting). To write the energy balance equation involved in our process, we consider an elementary volume dV at the surface of the material. The total quantity of heat accumulated in the element dV for a time dt is the sum of the energies accumulated by the three modes of heat transfer (conduction, convection, and radiation) and the absorbed energy on the surface of the metal object, which is induced by the laser:

$$dQ_{\text{tot}} = dQ_{\text{cond}} + dQ_r + dQ_{\text{conv}} + dQ_{\text{laser}}. \tag{1}$$

We assume that the intensity profile of the laser beam on the metallic surface is Gaussian and that it arrives at a normal incidence (in the $(\vec{dz})$ direction). The energy provided by the laser dQ_{laser} and absorbed by the surface $dS = dxdy$ during dt is given by the following:[26]

$$dQ_{\text{laser}} = \varphi_{\text{abs}} dSdt, \tag{2}$$

$$\varphi_{\text{abs}} = \alpha \frac{2P_{\text{in}}}{\pi r_0^2} e^{-2\left(\frac{x^2+y^2}{r_0^2}\right)}, \tag{3}$$

where φ_{abs} is the heat flux absorbed by the surface dS, α is the surface absorptivity for the laser wavelength, P_{in} is the incident power of the laser and r_0 is the radius of the laser beam at the focal plane. Exchanges by radiation and convection are considered to be losses for a surface element of the material dS, and therefore, we can write the following:[27]

$$dQ_r = -\varepsilon\sigma\theta^4 dSdt, \tag{4}$$

$$dQ_{\text{conv}} = -h_{\text{air}}(\theta - \theta_{\text{air}})dSdt, \tag{5}$$

where ε is the emissivity of the surface, σ is the Stefan-Boltzmann constant, θ is the temperature of the element dV, θ_{air} is the ambient temperature, and h_{air} is the heat transfer coefficient of the air during natural convection.

The quantity dQ_{cond}, which is accumulated in the elementary volume dV by conduction, can be calculated by Fourier's law, which gives the heat flow through a surface dS as a function of the temperature gradient:

$$dQ = -kdt\overrightarrow{\text{grad}}((\vec{\theta})) \cdot (\vec{\text{ds}}), \tag{6}$$

where k is the thermal conductivity of the studied material ($\text{W} \cdot \text{m}^{-1} \cdot \text{K}^{-1}$).

The conduction balance is then calculated using the above equation, according to the three dimensions of space. In our case, we can show that the total heat quantity accumulated by conduction in the element dV during the time dt is the following:

$$dQ_{\mathrm{cond}} = k\left(\frac{\partial^2\theta}{\partial x^2} + \frac{\partial^2\theta}{\partial y^2}\right)dVdt - k\frac{\partial\theta}{\partial z}dSdt. \tag{7}$$

Equation (1) describing the overall energy balance, becomes the following:

$$dQ_{\mathrm{tot}} = k\left(\frac{\partial^2\theta}{\partial x^2} + \frac{\partial^2\theta}{\partial y^2}\right)dVdt - k\frac{\partial\theta}{\partial z}dSdt - \varepsilon\sigma\theta^4 dSdt - h_{\mathrm{air}}(\theta - \theta_{\mathrm{air}})dSdt + \varphi_{\mathrm{abs}}dSdt. \tag{8}$$

The heat stored in an element dV causes a temperature rise according to the fundamental relation of the thermal physics, as follows:

$$dQ_{\mathrm{tot}} = \rho dV C_p \frac{\partial\theta}{\partial t}dt, \tag{9}$$

where ρ is the density of the material and C_p is its specific heat capacity.

For any element of the material surface, we have the following:

$$\rho C_p \frac{\partial\theta}{\partial t}dz = k\left(\frac{\partial^2\theta}{\partial x^2} + \frac{\partial^2\theta}{\partial y^2}\right)dz - k\frac{\partial\theta}{\partial z} - \varepsilon\sigma\theta^4 - h_{\mathrm{air}}(\theta - \theta_{\mathrm{air}}) + \varphi_{\mathrm{abs}}. \tag{10}$$

For any element within the volume, the losses by radiation and convection are removed (they are only surface phenomena), and the energy provided by the laser no longer affects the balance directly: $dQ_r = dQ_{\mathrm{conv}} = dQ_{\mathrm{laser}} = 0$. The exchange by conduction in the volume is uniform according to the three directions [Eq. (11)], and the overall equation becomes the classical heat equation [Eq. (12)].

$$dQ_{\mathrm{tot}} = dQ_{\mathrm{cond}} = k\left(\frac{\partial^2\theta}{\partial x^2} + \frac{\partial^2\theta}{\partial y^2} + \frac{\partial^2\theta}{\partial z^2}\right). \tag{11}$$

$$\rho C_p \frac{\partial\theta}{\partial t} = k\nabla^2\theta. \tag{12}$$

Solving Eqs. (10) and (12) for a 3-D problem is commonly performed using a finite element numerical solver (see below). If the thermophysical properties of materials are known or estimated, then it is possible to predict the optimal heating power for an SFH process. In the following simulation work, we assume that the heat transfer coefficient of air by free convection is $h_{\mathrm{air}} = 15\ \mathrm{W \cdot m^{-2} \cdot K^{-1}}$, a value usually estimated for air temperatures that are close to room temperature. The thermal conductivity is temperature-dependent, but we assume that its value is constant during the process because the temperature rise is relatively low. Many experimental databases are available in the literature. These values illustrate our problem, which concerns the extension of the SFH technique from glass to metal: $k = 250\ \mathrm{W \cdot m^{-1} \cdot K^{-1}}$ for aluminum and $k = 0.96\ \mathrm{W \cdot m^{-1} \cdot K^{-1}}$ for glass.[28] The coefficients α and ε depend on several parameters, such as the temperature, the incident angle φ and the wavelength λ. For the same reasons as mentioned above, we assume that the dependence on the temperature is negligible. The emissivity is the ratio between the quantity of energy that is emitted by a real body at a given temperature and the quantity of energy that would be emitted by a black body at the same temperature, given by Planck's law. According to Kirchhoff's law of thermal radiation, the directional spectral emissivity equals the directional spectral absorptivity. Additionally, the energy conservation principle for an opaque material specifies that the incident radiation is either reflected or absorbed (no transmission); the following equation results:[29]

$$\alpha_{\varphi,\lambda} = \varepsilon_{\varphi,\lambda} = 1 - \rho_{\varphi,\lambda}, \tag{13}$$

where $\rho_{\varphi,\lambda}$ is the bidirectional spectral reflectivity.

Many databases provide values for optical constants,[30,31] especially for metals in the IR spectral band.[32] For the case of metallic surfaces, we note that the directional emissivity is usually lower than for the dielectrics and is anisotropic because it increases for angles that are close to the tangent direction of the surface (Fig. 3).[33] This comment is especially true when the temperature increases, as shown in Fig. 4(a).[34] Therefore, these empirical data highlight equipment choice. When the observation wavelength decreases, the emissivity tends to increase, and it seems more useful to measure the emitted radiation in the near IR spectral band. As a consequence of Kirchhoff's law, if a body is a good emitter for a specific wavelength, then it is also a good absorber of that wavelength. To make the heating process application efficient, the laser wavelength must be small. The wavelength of our laser source will be chosen in the near IR range at 808 nm. A smaller wavelength would be outside the band of thermal interaction and would lead to other phenomena, such as ablation or fluorescence. Figure 4(b)[35] shows the wavelength-dependent spectral absorptivity of different metals, that is widely given in the literature.[36,37]

2.2 *Simulation Results*

According to these thermophysical properties, we propose a model for heat transfer that is described by Eqs. (10) and (12). The main purpose of the simulation is to predict the

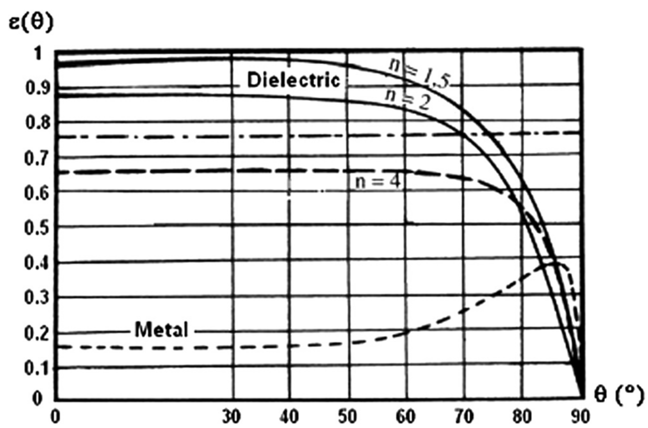

Fig. 3 Total directional emissivity for metals and dielectrics.

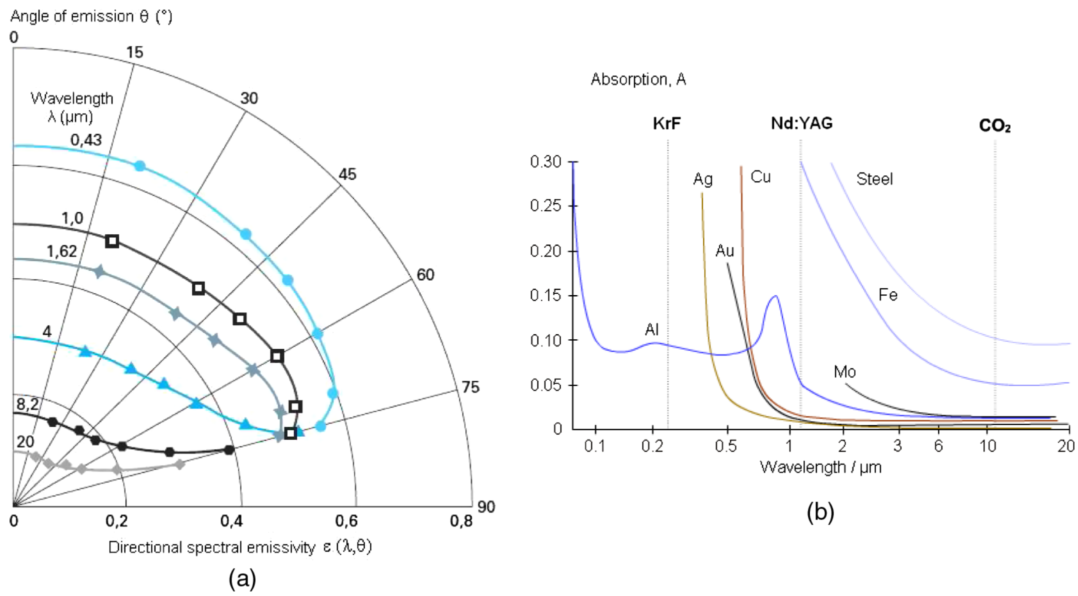

Fig. 4 (a) Directional spectral emissivity of titanium. (b) Absorptivity as a function of wavelength for different metals.

best settings for our heating system, the laser, for the SFH application on metallic surfaces. We use the method of finite element analysis to solve this problem in 3-D with the following conditions: the heating is provided at a normal incidence, at the center of the front side of a parallelepiped with a Gaussian beam of 0.5-mm radius, a wavelength of $\lambda = 0.808\ \mu$m, and a variable power, according to Eq. (3) (properties of the laser used for real experiments). The power flux deposited by the laser into the material is a square pulse in time, with a variable amplitude and duration. The medium is assumed to be semi-infinite, and the ambient temperature is 20°C. To measure a temperature difference detectable by a thermal camera, we set a minimal threshold to 3 K over the room temperature. In fact, the noise equivalent temperature difference (NEDT) of the used IR detector is $\sigma = 50$ mK at 30°C, which means that the probability that the measurement is not noise (Gaussian distribution of standard deviation σ) is 99.7% if the rise of apparent temperature measured on a black body is $6\sigma = 0.3$ K. We choose a factor of 10 to account for the difference in the emissivity of a metal and a black body.

As shown in Fig. 5, two situations could arise when estimating the settings of the laser source for a given material. In a case where the heating time is imposed (a fixed integration time of the camera, for example), the laser power is calculated such that the surface temperature can reach our detectability threshold of 3 K [see the examples in Fig. 5(a), for $t = 1$ ms, 10 ms, 20 ms]. In the opposite case, when the laser power is fixed, the rise time to 3 K is estimated for the material [Fig. 5(b)]. For example, these results predict that a 44.7 W minimum will be required to scan all of the materials that were presented in this example with a pulse duration of 1 ms. The rise times to 3 K are typically very short (less than 1 ms for $P = 50$ W), but increase rapidly if the power decreases, especially for highly conductive or barely absorbent materials. The following thermophysical properties are taken from the literature: thermal conductivity k, density ρ, specific heat capacity C_p, and absorptivity α for the considered wavelength.

Figure 6 shows the difference in the thermal field propagation after a laser pulse of 50 W during 0.5 sec at the surface of the steel and aluminum. However, this map represents only the real temperature on the object's surface. During the measurement of emitted radiation by an IR camera, the measured flux is given by Stefan's law and is proportional to the material emissivity for the sensitivity spectral band of the camera. Thus, the measure is an apparent temperature, which is different from the simulated temperature. This difference explains the limitations of the modeling and the high security factor chosen for the detectability threshold.

2.3 *Experimental System*

Relying on the simulation results, a 3-D scanner prototype has been implemented, based on the SFH technique. The system consists of a diode laser emitting at $\lambda = 808$ nm, and an IR imaging detector, which is sensitive to mid-wavelength IR (InSb quantum-based sensor for which the sensitivity spectral band extends from 1.5 to 5 μm). The system is fixed on a three-axis moving table, and the studied object is motionless in order to have a large scanning window (see Fig. 7). The working distance between the camera and the object is 60 cm and the focal length of the laser optics is 15 cm. The simulation results have shown that the thermal image should be acquired before the end of the laser pulse as the temperature drop is very fast. A programmable controller is used to synchronize the laser emission, the camera trigger, and the displacement of the table. Figure 8 compares the thermal response that is obtained by simulation with the measured response obtained by the IR camera for a laser pulse (15 W, 3 sec) on steel. The experimental results fit the theory reasonably well, even if the temperature rise is slower. This difference could be related to the difference in the physical properties of the standard steel chosen for the simulation and the real part (probably a greater diffusivity for the latter).

After setting the parameters of the laser source, the scanning procedure begins. For each intermediate position

(a)

	k (W/m.K)	ρ (kg/m³)	C_p (J/kg.K)	α	$P_{t=20ms}$ (W)	$P_{t=10ms}$ (W)	$P_{t=1ms}$ (W)
Oxidized steel	44,5	7850	475	0,3	**1,6**	**1,8**	**4,1**
Polished steel	44,5	7850	475	0,07	**7**	**7,8**	**17,5**
Oxidized aluminum	160	2700	900	0,25	**5,9**	**6,2**	**9,1**
Polished aluminum	160	2700	900	0,05	**29**	**31**	**44,7**
Oxidized Copper	400	8700	385	0,2	**18**	**18,4**	**24,5**
Tungsten	174	19300	130	0,4	**3,9**	**4,1**	**6,1**

(b)

	$t_{3K\ (P=50W)}$ (ms)	$t_{3K\ (P=30W)}$ (ms)	$t_{3K\ (P=10W)}$ (ms)
Oxidized steel	**0,025**	**0,034**	**0,15**
Polished steel	**0,12**	**0,3**	**3,9**
Oxidized aluminum	**0,03**	**0,06**	**0,8**
Polished aluminum	**0,715**	**13,9**	**9590**
Oxidized Copper	**0,125**	**0,45**	**2150**
Tungsten	**0,02**	**0,035**	**0,255**

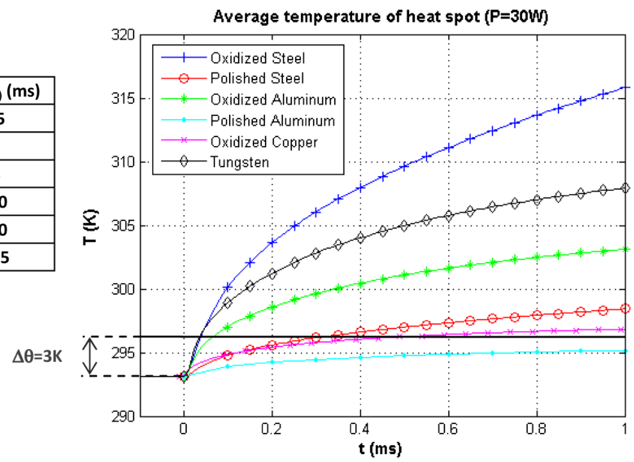

Fig. 5 (a) Powers predicted to reach 3 K after $t = 1$ ms, $t = 10$ ms, $t = 20$ ms; (b) Rise time to 3 K for different metals when $P = 10$ W, 30 W, 50 W and thermal response curves for $P = 30$ W.

(a)

(b)

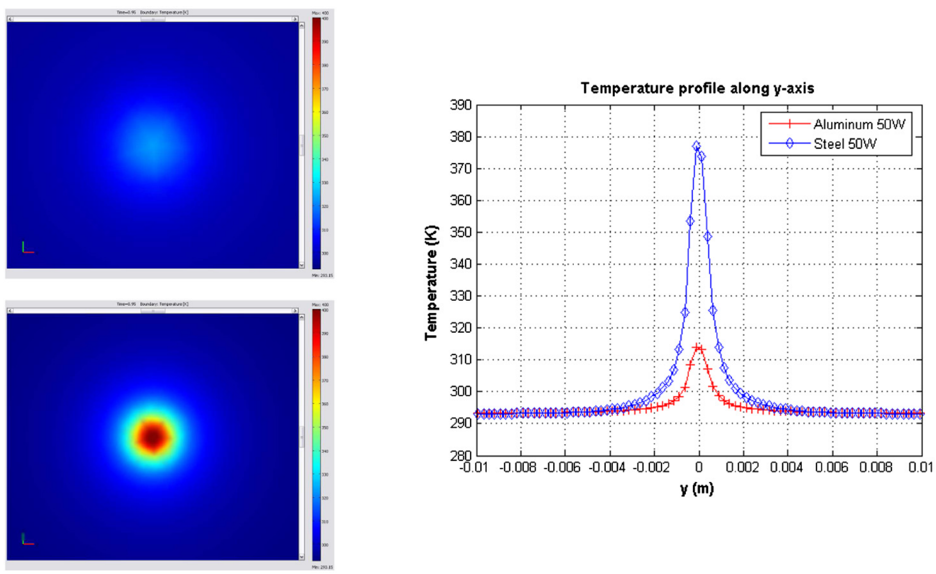

Fig. 6 Two-dimensional map and temperature profile for a Gaussian heating of 50 W during 500 ms on aluminum (a) and steel (b).

of the system, an image is acquired before and during the laser pulse to facilitate the position computation of the thermal spot in the images using background subtraction. Because the spatial resolution of IR cameras is typically poor (320×256 pixels, in our case), it will be necessary to apply a sub-pixellic method to obtain the maximum heat localization in the image frame. To perform this task, a Gaussian filter is applied to the image, and the heat spot is segmented by region-growing. Before the scan, a calibration step is performed to compute the relation between the position of the point in the image frame and the depth Z in the world-coordinate frame. Both the X and Y-coordinates are given by the moving table; thus, the calibration is based on measuring the position of the thermal spot when the laser is irradiating a plane placed at different depths Z_i. Then, the epipolar line provides a direct transformation between the image frame and the world frame, which is required for the computation of the 3-D coordinates of the considered

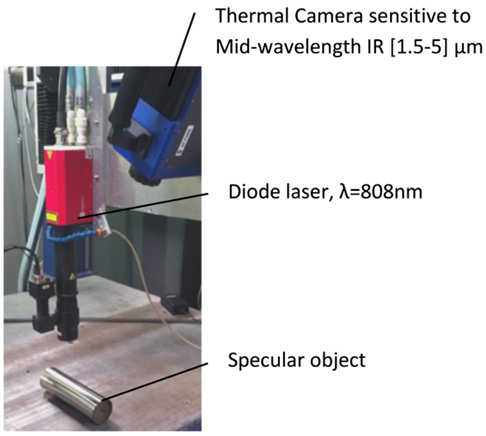

Fig. 7 Photo of the experimental setup.

point. Figure 9 presents the 3-D digitization results that were obtained for several specular objects with the system described above.

3 Influence of Roughness

3.1 *Preliminary Study*

Most of the authors mentioned in the introduction[8–15] based their scanning techniques on the assumption that the surface is specular, resulting in techniques that would not work on a diffuse surface. The proposed technique is based on the radiative properties of the materials, which means that if the heating source settings are adapted to the material then a surface could be digitized regardless of its roughness, specular or not. To demonstrate this invariance, an experiment is proposed to characterize the surface state influence by introducing the average roughness Ra in the study, which is defined in terms of international standards (ISO 4287). Ra is calculated by the arithmetical mean deviation of the profile within the reference length l, as follows:

$$R_a = \frac{1}{l}\int_0^l |Z(x)|\mathrm{d}x, \tag{14}$$

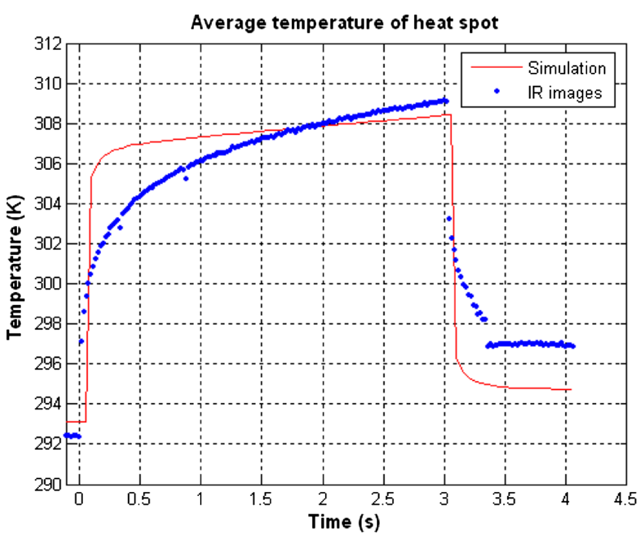

Fig. 8 Comparison of the simulated temperature with the measured temperature for steel.

where $|Z(x)|$ represents the absolute profile heights measured from the mean profile along the x-axis.

We can infer from Fig. 2 that roughness is directly related to specularity: the lower is the roughness, the higher is the proportion of the reflected radiation in the specular direction.

A simple experimental measurement can be performed to illustrate the dependence of the bidirectional reflectivity and the surface roughness [Fig. 10(a)]. Two steel objects with different roughness values are exposed to the radiation of a visible laser with an incidence angle of 30 deg and the intensity of a reflected ray is measured with a CCD camera. A specular spike with a few degrees of aperture appears clearly on the chart for the smoother surface (blue), whereas a wider reflected lobe is measured for the more diffuse surface. The equivalent measurement is performed in the band of thermal radiation [Fig. 10(b)]: a diode laser (NIR) and a thermal camera are used for the measurement of the IR emission. These results highlight the benefit of our technique because the radiation that is emitted in the IR band by a glossy or specular surface is omnidirectional and follows the reflectance model of a diffuse surface in the visible band (see Fig. 1).

A surface is defined as optically smooth if the surface irregularities are smaller than the wavelength of the incident ray. In fact, the roughness is not an intrinsic property of the material and, instead, depends on the working wavelength.[1] We must, therefore, choose roughness values that are sufficiently spread around the laser wavelength to define the diffuse and specular surfaces.

3.2 *Results and Discussion*

To efficiently compare the 3-D scanning results for different surface conditions, we used cylinders that were made of steel AISI 316L and that have identical dimensions but different average roughnesses [see Fig. 11(a)]. With various polishing techniques (mechanical or electrolytic), the Ra values we obtain range from 0.18 μm (electropolished) to 2.035 μm (blasted). The variation below and above the incident wavelength given by the laser at 0.808 μm is quite large.

As shown in Fig. 11(b), each cylinder is fastened onto an optical table with three aluminum spheres that will define a reference plane. To measure the deviation between two cylinder surfaces, the point clouds are first registered in this unique frame. The whole (the cylinder and the three spheres) is digitized by three systems: a touch-probe scanner (TPS), which will give the cloud of reference points by means of tactile measuring, a conventional scanner, which is based on a structured light projection (Steinbichler Comet 5), and our system, which is based on the SFH technique. For example, Fig. 12 shows the deviation map between the points that were digitized by each scanner and the reference points that were obtained from the touch-probe scanner on a surface with Ra = 1.35 μm.

Two main measurements distinguish the 3-D clouds that were computed by SFH from those given by the conventional scanner: the error distribution and the angle range. For the example above, the points are acquired with a standard deviation of 108 μm for the SFH, whereas the distribution error computed from the conventional acquisition result is 315 μm. In contrast, in the example presented in Fig. 12(b), the surface points for the SFH are acquired for

Fig. 9 3-D clouds of points digitized from specular surfaces.

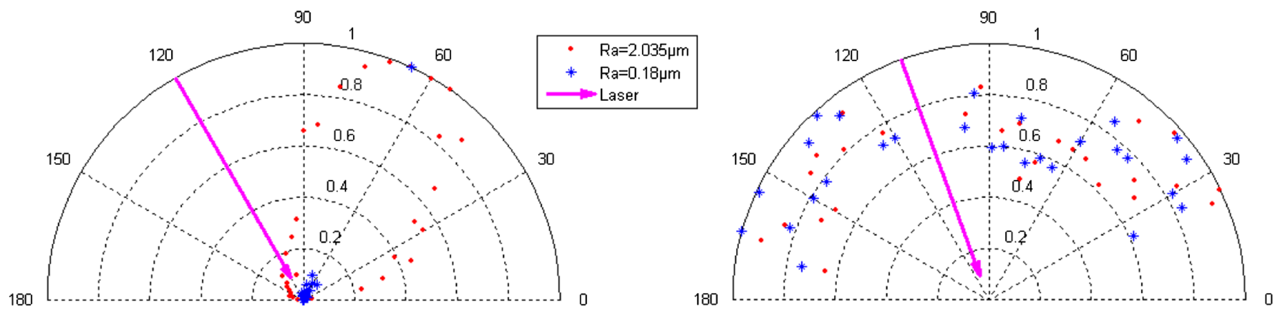

(a) (b)

Fig. 10 The bidirectional reflectance distribution for visible laser incidence (a) and the MWIR emission distribution for diode laser incidence (b) on two steels with different roughness values.

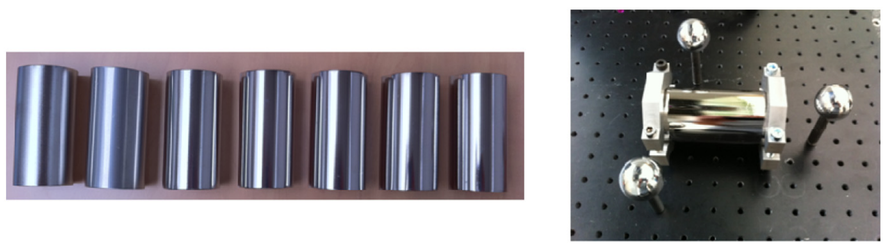

(a) (b)

Fig. 11 (a) Samples used for the study and (b) the experimental setup.

an incidence angle of up to $\alpha_{\max} = 62.2$ deg, with a total average error of 117 μm, whereas for the traditional system the maximum incidence angle is only $\alpha_{\max} = 10.8$ deg, with a greater total average error of 148 μm [Fig. 12(a)].

Concerning the eight samples, the overall average error is similar: 154 μm with the SFH-based scanner and 174 μm with the conventional scanner. Regarding the standard deviation of the error distribution, we notice significant

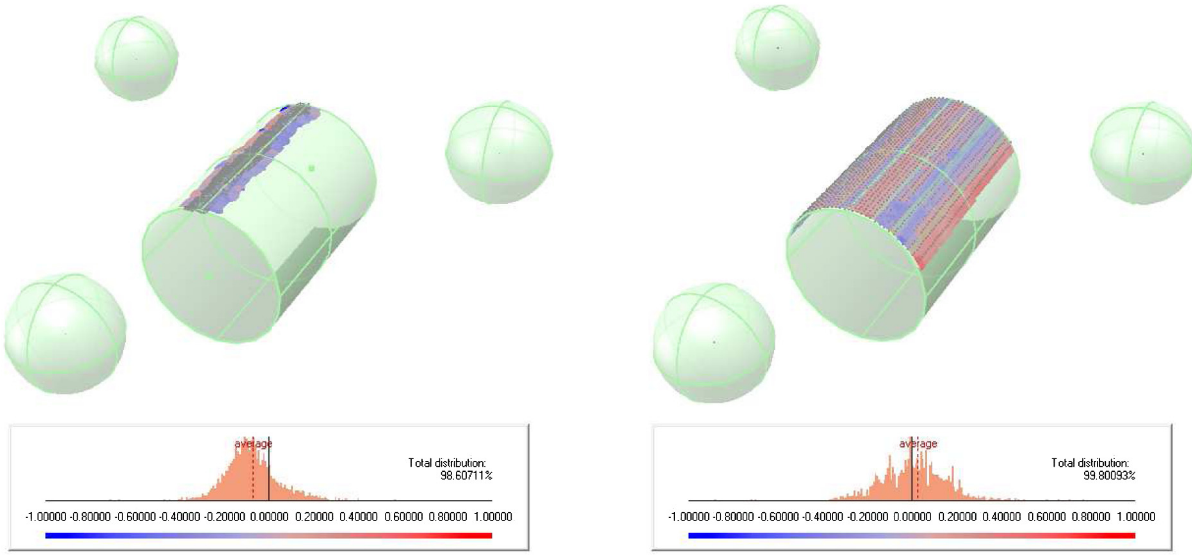

(a) (b)

Fig. 12 Deviation map and error distribution computed for the conventional scanner result (a) and for the SFH-based scanner result (b) (example of Ra = 1.35 μm).

Ref	Polishing process	Ra (µm)	σ(SFH-TPS) (mm)	σ(Comet-TPS) (mm)
1	Blasted	2.035	0.22627	0.20183
2	Blasted-electropolished	1.5444	0.13999	0.2753
3	Mechanical preparation	1.3534	0.10885	0.31509
4	Mechanical preparation ++	0.4042	0.15617	0.43769
5	Acid pickling	0.3014	0.13378	0.33521
6	Electropolished phase 1	0.2548	0.13167	0.38541
7	Electropolished phase 2	0.2256	0.14519	0.37545
8	Electropolished phase 3	0.1818	0.20912	0.38129

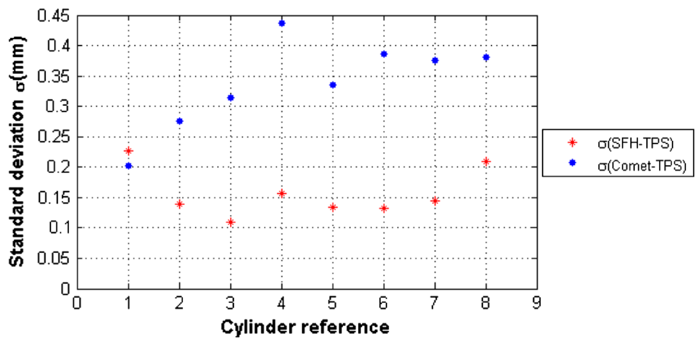

Fig. 13 Evolution of the standard deviation of the error distributions depending on the roughness for the two scanners.

Ref	α_{max} Comet	α_{max} SFH	$\varnothing_{TPS}$ (mm)	$\varnothing_{Comet}$-$\varnothing_{TPS}$ (mm)	$\varnothing_{SFH}$-$\varnothing_{TPS}$ (mm)
1	28.6°	69.8°	51.129	0.058	0.244
2	26°	55.3°	51.086	1.319	0.084
3	10.8°	62.2°	50.875	-7.269	-0.248
4	8.5°	62.2°	50.886	-	-0.229
5	14.6	65.3°	51.164	-4.014	-0.654
6	8.2°	61.6°	51.133	-1.279	-0.595
7	7.9°	62.2°	50.972	-5.284	-0.347
8	6.2°	62°	50.949	-11.197	-0.214

Fig. 14 Comparison of the maximum incidence angle authorized by the two scanners and the relative errors on the diameter measurement.

differences between the two systems (Fig. 13): with the SFH prototype, we obtain $\sigma = 156$ μm (average for the eight measurements), and we obtain $\sigma = 338$ μm for the Comet scanner. For the visible system, the error tends to disperse when the roughness decreases, which is not true for the IR system. Furthermore, we observe a relative stability in the standard deviation values because the maximum variation of σ is 117 μm with our method versus 235 μm with the conventional system. Nevertheless, the error histogram shows that the errors given by the SFH are not uniformly distributed around zero. This problem could be caused by mechanical vibrations in the scanning direction or by a

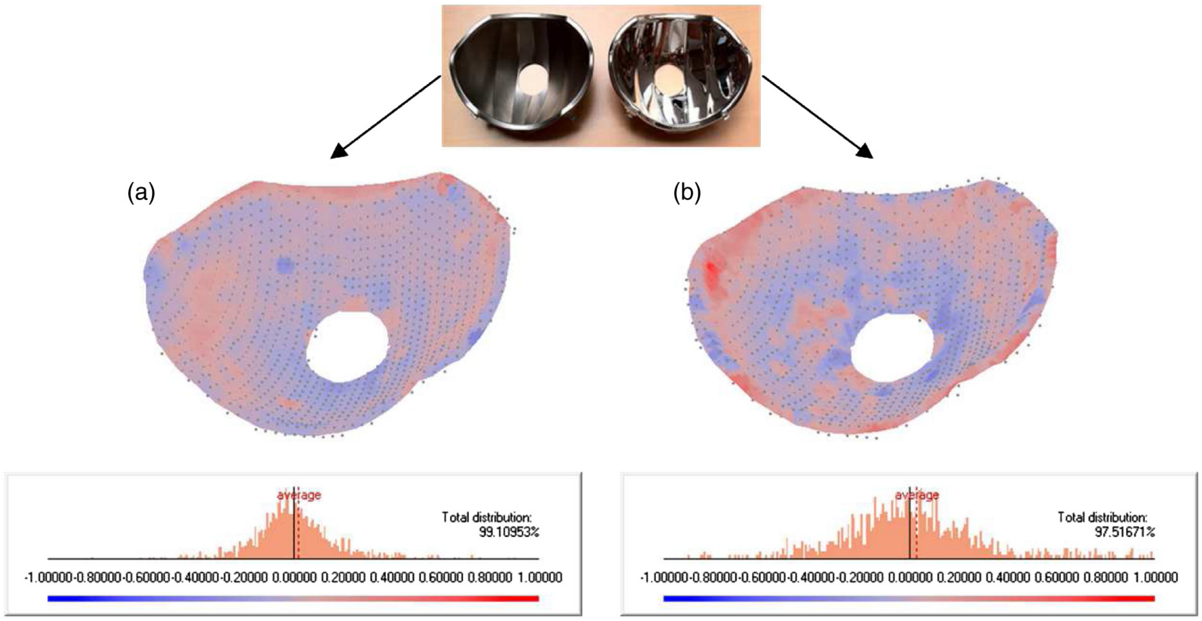

Fig. 15 Comparison of 3-D scanning results on (a) a glossy workpiece (Ra = 1.066 μm) and on (b) a specular workpiece (Ra = 0.094 μm).

default in the geometric quality of the laser beam. Asymmetry in the energy distribution has been measured at the focal plane of the laser and could distort the detection of the heat point. Furthermore, because of the low spatial resolution of the thermal sensor, it could influence the 3-D coordinate computation of the point, depending on the position of the beam on the work piece.

Nevertheless, the main issue regarding these acquisitions concerns the width of the point clouds. According to the summary table given in Fig. 14, the angle of incidence reaches only 28.6 deg in the case of the Comet scanner for the most diffuse surface, while it remains quite stable around an average of 63 deg for the SFH scanner. Figure 14 also shows another measurement: the cylinder diameters are estimated from the digitized cloud of points. For an application that would require the determination of the diameter of the cylinder, the average error in the measurement would be 3.952 mm for the visible scanner and 0.245 mm for the SFH-based scanner.

Overall, the size of the clouds of points acquired and the standard deviation of the error distribution are not related to the surface roughness for the studied samples, which is in contrast to a conventional scanner. Thus, we have shown the feasibility and the efficiency of our method on diffuse, glossy and specular metallic surfaces. However, the evaluated measurement accuracies depend on the quality of the registration [the fitting obtained from the three reference spheres' digitization, shown in Fig. 11(b)] and are also related to the cylindrical shape of the samples. A metrological study would be necessary to improve the evaluation of the global error of our prototype.

3.3 *Industrial Issues*

The results presented in Fig. 15 correspond to a real issue for an automotive equipment manufacturer that produces reflectors for car lights. Three-dimensional maps show the deviation between the point cloud that is digitized by the SFH technique and a reference model that is obtained by a conventional scanner and applied to the powdered parts. The calculated average errors are 135 μm on the diffuse reflector [Fig. 15(a)] and 235 μm on the specular reflector [Fig. 15(b)]. Due to the mechanical displacement, the acquisition process is relatively long, and the density of the point cloud is not very high (1720 points per scan). For this reason, the error is mainly localized on the reflectors' edges, where the step of the scanning is not narrow enough. The major difficulty in this example is that the specular work piece is covered with a protective layer of polymer that compels us to limit the laser power (damage risk). While the reflection losses are greater than for the diffuse surface, the laser power used is the same (20 W), which complicates the heat point detection and justifies the greater error on this reflector. The histograms also reveal the difference in standard deviation between the two error distributions: $\sigma_{\text{rough}} = 169$ μm and $\sigma_{\text{specular}} = 250$ μm. However, once again the size of the 3-D point cloud does not vary between the diffuse surface and the specular surface. The complete point clouds have been computed in only one direction of acquisition, in contrast to conventional scanners for which several points of view are sometimes required to complete the surface acquisition.

4 Conclusions and Future Research

Through the study of thermophysical properties of metals and the modeling of the thermal problems, we have shown that a laser and an IR camera can be set up to digitize metallic specular surfaces in 3-D. Unlike other experimental methods of acquisition that are based only on the specularity interpretation of visible light, the system we propose can operate with similar performances on diffuse and specular surfaces (classes A, B and C, as identified in Fig. 1). To estimate the accuracy of our prototype, we compared our 3-D digitization results with the results obtained using a commercial active scanner on surfaces of identical dimensions but varying roughness. The average error of measurement (154 μm) is similar to measurements resulting from a conventional scanner acquisition (174 μm). However, the standard deviation of the error distribution is lower and does not change significantly with the roughness, whereas for the conventional scanner, it increases rapidly with the specularity. Furthermore, the angle range of the acquired cloud of points is greater with our IR system. In fact, with a similar error between the two systems for the most specular surface, a 3-D point can be computed with an incidence angle of up to 62 deg with our system and only up to 6 deg for the other system.

The proposed technique could be inoperative for surfaces that have a specular reflectance that is perfect for any wavelength of an existing laser. In other words, if the absorptivity value is always zero (a theoretically non-existing case), then it is impossible to heat the surface by means of radiation. We also have seen that knowledge, or at least an estimation of the thermophysical properties of the work material, is required to apply the SFH technique. In the case of a heterogeneous material, a procedure of self-adjustment of the laser intensity would be required.

The main perspectives of this study rely on the optical and mechanical optimization of the experimental setup and on the implementation of a new system that is based on IR structured light projection. The prototype presented in this paper is quite slow because of the mechanical displacement of the whole system, and pattern projection would improve both the accuracy and the speed of scanning.

Acknowledgments

In the context of this study, we would like to especially thank Company Poligrat France Sud, 2 rue Saint-Eloi—F 71300 MONTCEAU-LES-MINES. LTm research team (Laser et Traitement des matériaux) from IRM Department of Laboratoire ICB, UMR 5209 CNRS-Université de Bourgogne, 12 Rue de la Fonderie—F 71200 LE CREUSOT, especially Pr. P. Sallamand. Partners from “3-DSCAN” European project.

References

1. S. K. Nayar, E. Ikeuchi, and T. Kanade, *Surface Reflection : Physical and Geometrical Perspectives* Robotics Institute, Pittsburgh, PA, CMU-RI-TR-89-07 (1989).
2. G. Sansoni, M. Trebeschi, and F. Docchio, “State-of-the-art and applications of 3-D imaging sensors in industry, cultural heritagen medicine, and criminal investigation,” *Sensors* **9**(1), 568–601 (2009).
3. F. Chen, G. M. Brown, and M. Song, “Overview of three-dimensional shape measurement using optical methods,” *SPIE Opt. Eng.* **39**(1), 10–22 (2000).
4. J-A. Beraldin et al., “Active 3-D sensing,” *Modelli E Metodi Per Lo Studio E La Conservazione Dell’Architecttura Storica* **10**, 22–46 (2000).
5. F. Blais, “Review of 20 years of range sensor development,” *J. Electron. Imag.* **13**(1), 231–240 (2004).
6. F-W. Bach et al., “Non-Contact geometry inspection of workpieces with optically non-cooperative surfaces,” *Key Eng. Mater.* **438**, 123–129 (2010).
7. I. Ihrke et al., “Transparent and specular object reconstruction,” *Comp. Graph. For.* **29**(8), 1–27, Blackwell Publishing, UK, USA (2010).
8. J. Park and A. C. Kak, “3-D modeling of optically challenging objects,” *IEEE Trans. Vis. Comput. Graphics.* **14**(2), 246–262 (2008).
9. L. B. Wolff and T. E. Boult, “Constraining object Features using a polarization reflectance model,” *IEEE Trans. Pattern Anal. Mach. Intell.* **13**(7), 635–657 (1991).
10. S. Rahmann and N. Canterakis, “Reconstruction of specular surfaces using polarization imaging,” in *IEEE Computer Vision and Pattern Recognition*, Kauai, USA, pp. 149–155 (2001).
11. O. Morel et al., “Active lighting applied to 3-D reconstruction of specular metallic surfaces by polarization imaging,” *Appl. Opt.* **45**(17), 4062–4068 (2006).
12. M. Tarini et al., “3-D Acquisition of mirroring objects,” *Graph. Models.* **67**(4), 233–259 (2005).
13. T. Bonfort, P. Sturm, and P. Gargallo, “General specular surface triangulation,” *Asian Conf. Computer Vision* **II**, 872–881 (2006).
14. J. Y. Zheng and A. Murata, “Acquiring 3-D object models from specular motion using circular lights illumination,” in *IEEE Int. Conf. Computer Vision* Bombay, pp. 1101–1108 (1998).
15. J. Y. Zheng and A. Murata, “Acquiring a complete 3-D model from specular motion under the illumination of circular-shaped light sources,” *IEEE Trans. Pattern Anal. Mach. Intell.* **22**(8), 913–920 (2000).
16. D. N. Bhat and S. K. Nayar, “Stereo and specular reflection,” *Int. J. Comput. Vision* **26**(2), 91–106 (1998).
17. M. Gupta, A. Agrawal, and A. Veeraraghavan, “Structured light 3-D scanning in the presence of global illumination,” in *IEEE Conf. Computer Vision Pattern Recognition (CVPR)* Providence, RI, pp. 713–720 (2011).
18. R. Rantoson, Numérisation 3-D d’objets transparents par polarisation dans l’IR & par triangulation dans l’UV, Université de Bourgogne, Thèse (2011).
19. H. J. Tiziani and H. M. Uhde, “Three-dimensional image sensing by chromatic confocal microscopy,” *Appl. Opt.* **33**(10), 1838–1843 (1994).
20. Nikon Metrology. Web Site—Handheld 3-D scanners. [Online]. HYPERLINK “http://www.nikonmetrology.com/handheld_scanners/mmdx_mmc/”.
21. J. L. Bodnar and M. Egée, “Wear Crack characterization by photothermal radiometry,” *WEAR* **196**(1–2), 54–59 (1996).
22. J.-F. Pelletier and X. Maldague, “Shape from heating: a two-dimensional approach for shape extraction in infrared images,” *Opt. Eng.* **36**(2), 370–375 (1997).
23. J.-J. Orteu et al., “An innovative method for 3-D shape, strain and temperature full-field measurement using a single type of camera: principle and preliminary results,” *Exper. Mechan.* **48**(2), 163–179 (2008).
24. G. Eren et al., “Scanning from heating: 3-D shape estimation of transparent objects from local surface heating,” *Opt. Express* **17**(14), 11457–11468 (2009).
25. G. Eren, 3-D Scanning of Transparent objects, Université de Bourgogne—Sabancı Üniversitesi, Thèse de doctorat, (September 2010).
26. R. Paschotta, *Gaussian Beams* Encyclopedia of Laser Physics and Technology RP Photonics Consulting GmbH (Virtual Library) (2011).
27. B. Eyglunent, *Manuel de Thermique* Hermès Science Publication Paris (2000).
28. The Engineering ToolBox. Thermal Conductivity of some common Materials and Gases. [Online]. “http://www.engineeringtoolbox.com/thermal-conductivity-d_429.html”.
29. Fred E. Nicodemus, “Directional Reflectance and Emissivity of an Opaque Surface,” *Electronic Defense Laboratories* Defense Documentation Center for Scientific and Technical Information California (1965).
30. Edward D. Palik, *Handbook of Optical Constants of Solids* Academic Press, Boston (1985).
31. Y. S. Touloukian, *Thermophysical Properties of Matter* Springer (1995).
32. M. A. Ordal et al., “Optical properties of the metals Al, Co, Cu, Au, Fe, Pb, Ni, Pd, Pt, Ag, TI, and W in the infrared and far infrared,” *Appl. Opt.* **22**(7), 1099–1119 (1983).
33. G. Gaussorgues, *Infrared Thermography*, Chapman & Hall, London (1994).
34. D. K. Edwards and I. Catton, “Radiation characteristics of rough and oxidized metals,” *Adv. Thermophys. Proprieties Extreme Temp. Pressures* 189–199 (1965).
35. University of LiverpoolMATTER. Alu-matter. [Online]. “http://aluminium.matter.org.uk” (2010).
36. B. Karlsson and G. Ribbing, “Optical constants and spectral selectivity of stainless steel and its oxides,” *J. Appl. Phys.* **53**(9), 6340–6346 (1982).
37. S. B. Boyden and Y. Zhang, “Temperature and wavelength-dependant spectral absorptivities of metallic materials in the infrared,” *J. Thermophys. Heat Trans.* **20**(1), 9–15 (2006).

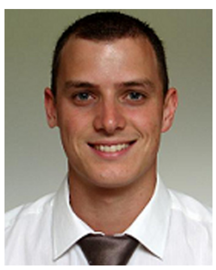

Alban Bajard received his MS engineering degree in “optics and industrial vision” from TELECOM Saint-Etienne and Jean Monnet University of Saint-Etienne, France in 2009. He is currently working towards a PhD at Le2i (3-D Vision team), Unité Mixte de Recherche, Centre National de la Recherche Scientifique 5158, University de Bourgogne. He is working on 3-D digitization of metallic surfaces, especially specular and highly reflective objects.

Olivier Aubreton received the aggregation examination in 2000 and the DEA degree (equivalent to a MS) in image processing in 2001. Since September 2005, he has been an assistant professor with the Laboratory Le2i (Vision 3-D team), Institut Universitaire de Technologie, Le Creusot, France. His research interests include the design, development implementation, and testing of silicon retinas for pattern matching and pattern recognition. He is currently working on the development of new solutions for 3-D reconstruction of problematic surfaces (specular and transparent objects) and the development of 3-D processing approaches for salient point detection on 3-D meshes.

Youssef Bokhabrine received a MSc degree in computer vision and image processing in 2006 and PhD degree in computer vision in October 2010, both from the University of Burgundy, France. He is currently a postdoctoral researcher at laboratory LE2I, University of Burgundy. His research interests are in the field of machine vision and 3-D reconstruction.

Benjamin Verney received his BS in optics and photonics in 2010 at Grenoble, France. He is currently undergoing an apprenticeship towards his engineering degree in "optics and industrial vision" from TELECOM Saint-Etienne of Jean Monnet University, Saint-Etienne, France. He currently works for Welience, affiliated with Ub in R&D of 3-D Scanning systems dedicated to reflective surfaces along with the Le2i (3-D Vision Team), Unité Mixte de Recherche, Centre National de la Recherche Scientifique 5158, University de Bourgogne.

Gönen Eren received BS and MS degrees in computer engineering from Galatasaray University, Istanbul, Turkey, in 2004 and 2007, respectively. He received a double PhD degree in Computer Science from Sabanci University, Istanbul, and the University of Burgundy, Dijon, France. He is currently an assistant professor at Galatasaray University Computer Engineering Department. His research interests are machine vision, robotics and interactive art.

Aytül Erçil received BS degrees in electrical engineering and in mathematics from Boğaziçi University, Istanbul, Turkey, in 1979 and the MS and PhD degrees in applied math from Brown University, Providence, Rhode Island, U.S. in 1980 and 1983, respectively. She is currently with the faculty of Engineering and Natural Sciences, Sabancı University, Istanbul, where she is the Founding Director of VPALAB, which was selected by the European Union as a "potential center of excellence." She is the founding president of the Turkish Pattern Analysis and Image Processing Group. Her specific research interests include invariant object recognition, shape modeling, texture analysis, biometrics, and image segmentation. She has directed many national and international projects (Nato, FP4, Eureka, NSF, FP6, Nedo) and is the founding partner and chief executive officer of a spin-off company Vistek A.¸ S.

Fred Truchetet received an MS in physics in 1973 and a PhD in electronics in 1977 from Dijon University, France. He worked at Thomson-CSF for two years as a research engineer and I was aboratory head for electronics, image and computing at (Le2i) of Université de Bourgogne for four years. He is currently "Professeur des Universités" in Le2i, UMR CNRS 5158, vice president of the Université de Bourgogne. His research interests are focused on image processing for artificial vision inspection and particularly on wavelet transform, multi-resolution edge detection and image compression. He has authored and co-authored more than 200 international publications, including 52 journal papers, three textbooks and holds four patents. He is a member of SPIE, a former chairman of SPIE's conference on wavelet applications in industrial processing, chairman of SPIE's conference on Optics, Photonics and Digital Technologies for Multimedia Applications and a member of numerous technical committees of international conferences in the area of computer vision.